RESEARCH PAPER

Channels 7:6, 503–513; November/December 2013; © 2013 Landes Bioscience

Cav1.4 IT mouse as model for vision impairment in human congenital stationary night blindness type 2

Dagmar Knoflach[1], Vasily Kerov[2,8], Simone B Sartori[3], Gerald J Obermair[5], Claudia Schmuckermair[3], Xiaoni Liu[2], Vithiyanjali Sothilingam[4], Marina Garcia Garrido[4], Sheila A Baker[8], Martin Glösmann[7], Klaus Schicker[1], Mathias Seeliger[4], Amy Lee[2], and Alexandra Koschak[1,*]

[1]Medical University Vienna; Centre for Physiology and Pharmacology; Department of Neurophysiology and Pharmacology; Vienna, Austria; [2]University of Iowa; Department of Molecular Physiology & Biophysics; Iowa City, IA USA; [3]University of Innsbruck; Institute of Pharmacy, Pharmacology and Toxicology; Center for Chemistry and Biomedicine; Innsbruck, Austria; [4]University of Tübingen, Institute for Ophthalmic Research; Centre for Ophthalmology; Division of Ocular Neurodegeneration; Tübingen, Germany; [5]Medical University Innsbruck; Division of Physiology; Innsbruck, Austria; [6]Department of Histology and Institute of Bioengeneering; Universidad Miguel Hernández; Alicante, Spain; [7]University of Veterinary Medicine; Vetcore; Vienna, Austria; [8]University of Iowa; Department of Biochemistry; Iowa City, IA USA

Keywords: CSNB2, L-type calcium channel, channelopathies, gain-of-function, retinal

Mutations in the *CACNA1F* gene encoding the Cav1.4 Ca^{2+} channel are associated with X-linked congenital stationary night blindness type 2 (CSNB2). Despite the increasing knowledge about the functional behavior of mutated channels in heterologous systems, the pathophysiological mechanisms that result in vision impairment remain to be elucidated. This work provides a thorough functional characterization of the novel IT mouse line that harbors the gain-of-function mutation I745T reported in a New Zealand CSNB2 family.[1] Electroretinographic recordings in IT mice permitted a direct comparison with human data. Our data supported the hypothesis that a hyperpolarizing shift in the voltage-dependence of channel activation—as seen in the IT gain-of-function mutant[2]—may reduce the dynamic range of photoreceptor activity. Morphologically, the retinal outer nuclear layer in adult IT mutants was reduced in size and cone outer segments appeared shorter. The organization of the outer plexiform layer was disrupted, and synaptic structures of photoreceptors had a variable, partly immature, appearance. The associated visual deficiency was substantiated in behavioral paradigms. The IT mouse line serves as a specific model for the functional phenotype of human CSNB2 patients with gain-of-function mutations and may help to further understand the dysfunction in CSNB.

Introduction

Cav1.4 L-type Ca^{2+} channels (LTCCs) are the most abundant in the retina and localized at the specialized ribbon synapses formed between photoreceptors and second-order neurons.[3,4,5,6] Their low voltage activation range and slow inactivation properties due to the lack of calcium-dependent inactivation[7] render Cav1.4 channels perfectly suited to ensure sustained neurotransmitter release which is modulated by light stimuli.

Human genetic analyses indicate an essential role for Cav1.4 in vision. So far, more than 50 different mutations in *CACNA1F*, the gene coding for the Cav1.4 channel, have been found to cause congenital stationary night blindness type 2 (CSNB2) in human patients (for review see ref. 8). The majority of mutations are predicted to form non-functional channels, often because of structural changes like premature truncations that are incompatible with channel function. However, also gain-of-function mutations have been reported and characterized biophysically in transfected mammalian cells or *Xenopus* oocytes.[2,9,10,11] Data on functional implications in their native retinal environment remain still scarce. Cav1.4 gain-of-function mutations promote enhanced Ca^{2+} entry through the channel due to a strong hyperpolarizing shift in the voltage-dependence of activation which as well as slowed voltage-dependent inactivation. The so far most pronounced hyperpolarizing shift in Cav1.4 channel activation (around 30 mV) was found in mutation I745T (IT), which was identified in a New Zealand family. The affected family members were described to show an unusually severe CSNB2 phenotype—usually comprising low visual acuity, myopia, nystagmus, and variable levels of night blindness (clinically diagnosed by a reduction in the ERG b-wave)—which was associated with intellectual disability in males. In heterozygote females, clinical and functional abnormalities were also present.[2] 'Enhanced activity', as observed in gain-of-function mutations, implies an unwarranted positive connotation because it does not necessarily result in improved signaling but in a loss-of-control of existing signaling pathways important e.g., in developmental processes. Herein, we present the functional dysregulation and morphological consequences observed in retinas from IT mice. These findings correlate with impaired visual function in behavioral paradigms seen in these mice. Our data show that the IT mouse line, in contrast to

*Correspondence to: Alexandra Koschak; Email: alexandra.koschak@meduniwien.ac.at
Submitted: 08/30/2013; Accepted: 09/03/2013
http://dx.doi.org/10.4161/chan.26368

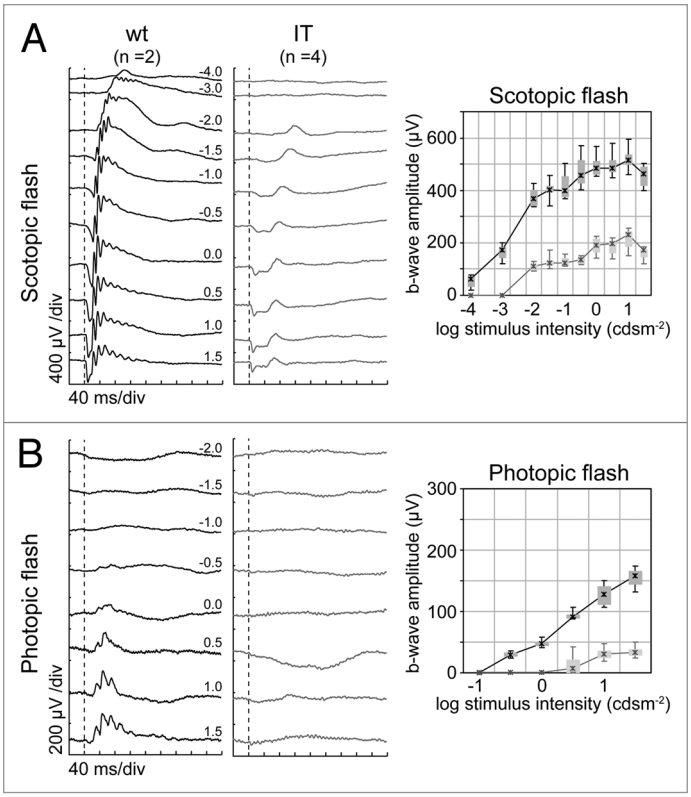

Figure 1. Functional assessment of wt and IT mouse retinas in vivo based on ERG. Left column: Representative Ganzfeld-ERG intensity series for dark-adapted (scotopic, [**A**]) and light-adapted (photopic, [**B**]) responses in wt (black) and IT mice (gray). Right column: Quantitative evaluation of the scotopic (**A**) and photopic (**B**) b-wave amplitude data for the entire group (wt, n = 2; IT, n = 4).

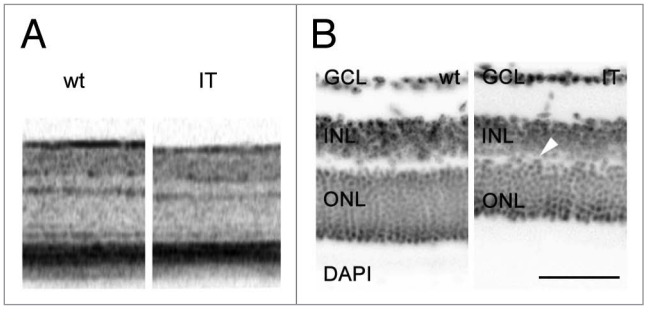

Figure 2. Morphological assessment of wt and IT mouse retinas. (**A**) In vivo OCT analysis of wt and IT mouse retinas, indicating (i) a reduction of the photoreceptor-containing outer nuclear layer (ONL), and (ii) a less expressed patterning of the inner/outer segment (IS/OS) border. (**B**) Retinal slices of adult wt (left) and IT (right) mice were stained with DAPI to show the nuclei. Light microscopic pictures from wt and IT were aligned at the GCL. Exemplar sections were taken from slices showing the same eccentricity. The reduction in the thickness of the ONL and INL in IT mice is evident (in [µm] for wt and IT respectively: ONL: 56 vs. 35; INL: 37 vs. 22). The arrow indicates the obvious misorganisation of the OPL. ONL, outer nuclear layer, INL, inner nuclear layer, GCL, ganglion cell layer. Scale bar 50 µm.

other mouse models characterized so far,[12] very well reflects the functional phenotype described in a family with the Cav1.4 I745T point mutation.[1]

Results

Rod and cone photoreceptor activity in wt and IT mice

Ganzfeld ERG recordings allow both dark adapted (scotopic) measurements to study rod-driven activity and light adapted (photopic) recordings to obtain information about the contribution of the cone system.[16] We found that adult IT animals very well matched their human CSNB2 counterparts in terms of the functional pattern resembling incomplete CSNB. Both rod and cone single flash responses (**Fig. 1A and B**) as well as the flicker ERG amplitude (not shown) were reduced. In contrast, the negative components of the scotopic standard flash response were smaller than those found in other CSNB models, and a minute but distinct positive peak indicated a remaining b-wave component. However, identical differences were found in patients carrying the exact same mutation.[1] The IT mouse line is therefore a representative model for human CSNB2 caused by the I745T mutation.

Morphological characteristics in Cav1.4 wild type (wt) and IT mouse retinas

Optical coherence tomography (OCT) of retinal substructures/layers in vivo indicated a distinct reduction in the outer plexiform layer (OPL) thickness in the mutant mice (**Fig. 2A**). This finding is in line with our histomorphological analysis (**Fig. 2B**). Specifically, a DAPI staining was performed on retinal sections of adult (2 mo-old) mice to compare the thickness of the retina as well as that of the major retinal layers at three different eccentricities in wt and IT. At comparable eccentricities, the rows of nuclei in the outer nuclear layer (ONL) were counted. Gross retinal structure and layering were normal in IT mice. All retinal layers were present. However, the number of rows of nuclei in the ONL was lower in IT than in wt mice resulting in a reduction in the thickness of the ONL and the total retinal thickness (**Fig. 2B**). OCT further revealed a less expressed patterning of the inner/outer segment (IS/OS) border that is indicative of irregular outer retinal layering (**Fig. 2A**).

We assessed potential aberrations in cone morphology by labeling with peanut agglutinin (PNA), a lectin preferentially binding cone-photoreceptor associated domains of the interphotoreceptor matrix[30,31] and glycogen phosphorylase (glypho), which stains cones from their outer segments to their pedicles.[32] PNA labeling demonstrated that outer segments were present and of normal appearance (**Fig. 3A**). However, and in accordance with the decreased thickness of the ONL, the overall length of cones was shorter in IT mice. PNA-positive pedicles were also observed in the IT retina (**Fig. 3A**, arrowheads), with no obvious dissimilarity to the wt retina. No decrease in the number of cones was evident (as also indicated in **Fig. 4C**). In the wt retina anti-glypho stained the inner segments of cone photoreceptors, known sites of high energy consumption, as well as cone pedicles (**Fig. 3B**, left). Cone photoreceptors in IT mice were shorter with shorter outer and inner segments and pedicles that appeared larger than in wt retina

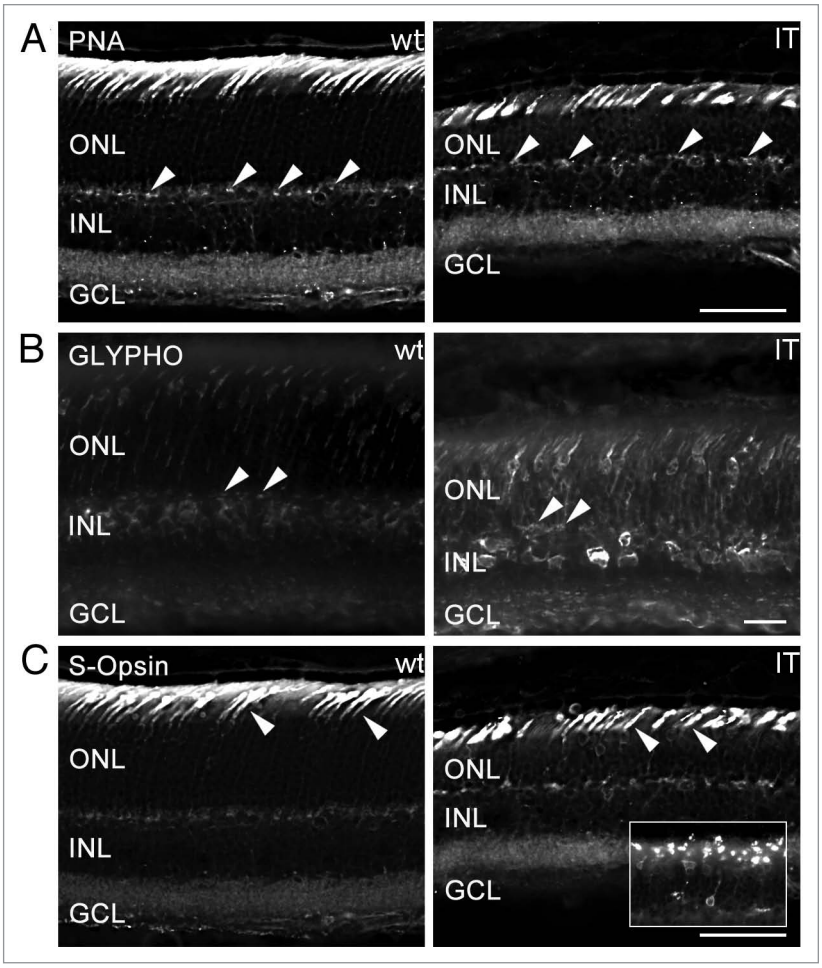

Figure 3. Effect of the IT mutation on adult mouse cones. Immunohistochemical analyses were performed on P74–81 (11-week old mice) mice using cone-specific markers and vertical sections were analyzed by wide-field fluorescence light microscopy. (**A**) PNA staining shows cones with normal appearance but shorter outer segments. Arrowheads indicate comparable staining of cone pedicle invaginations in wt (C57BL/6N) and IT mice. Scale bar 50 µm (**B**) Glypho also strongly labels the cone terminals. In IT mice immunostaining was pronounced throughout the cytoplasm from the outer segment to the synaptic pedicle. Arrowheads indicate enlargement of pedicles. Scale bar 20 µm. (**C**) S-opsin staining experiments for wt and IT retinas. The inset shows a sprouted cone (left), a mislocalized cone cell body (middle) and an enlarged cone pedicle (right). Scale bar 50 µm.

(**Fig. 3B**, right, arrowheads). Notably, glypho signal was consistently higher in the IT mutant, both in the inner and outer retina. Using the S-opsin marker sc14363 we found S-opsin expression clearly visible in the cone outer segments in the ventral wt retina as well as their pedicles (**Fig. 3C**, left). Consistent with our glypho staining cones were shorter in IT mice (**Fig. 3C**, right, arrowheads). As seen in the inset of **Figure 3C**, indeed we found a few cones that appeared to sprout, a phenomenon seen also in KO mice at different ages.[33]

We further examined the photoreceptor synaptic phenotype and investigated Cav1.4 expression in co-localization experiments with the synaptic ribbon protein CtBP2/Ribeye in wt and IT mice (**Fig. 4**). In adult wt retina, Cav1.4 co-localized in the characteristically horseshoe-shaped synapses in the OPL, whereas in IT retinas staining was disperse extending also into the ONL. The synaptic morphology resembled immature synapses with shorter but rather linear shape; in some ribbons elongated or regular horseshoe appearance was preserved (**Fig. 4A**). Immunofluorescence with the bipolar cell marker PKC-α also demonstrated the presence of ectopic synapses that were protruding into the ONL of IT retinas whereas in wt mice no sprouting of rod bipolar dendrites was observed (**Fig. 4B**). Ribeye/PNA co-staining was comparable in wt and IT retinas (**Fig. 4C**).

Expression profile of calcium channels in wt and IT mouse retinas

To test whether the insertion of a mutation in the *CACNA1F* gene induced changes in the expression of other Cav channel subunits we performed qRT-PCR experiments from adult wt and IT mice. All Cav α_1 subunits except Cav1.1 were reliably expressed in IT mouse retinas, although at different expression levels (**Fig. 5**). Cav1.4, β_2, and $\alpha_2\delta$-4 were by far the most abundantly expressed isoforms in IT mice. Even though suggested from previous independent publications[34,35] this finding has not been shown before in direct comparison using the same tissue samples. The total amount of calcium channel transcripts in IT mice was not significantly different from wt but an approximately 25% reduction in the expression of Cav1.4

Table 2. Behavioral measures assessed in diverse tests of anxiety in wt and IT mice. Data are presented as means ± SEM

	wt, n = 13	IT, n = 11	Student t test	
Open field test			t value	p value
center entries (n)	34 ± 2	41 ± 4	1.230	0.232
center time (s)	143 ± 15	132 ± 15	0.499	0.623
distance traveled (cm)	2634 ± 105	2873 ± 160	1.284	0.213
Elevated plus maze				
latency to first open arm entry (s)	23 ± 4	18 ± 3	10.861	0.401
open arm entries (n)	9 ± 1	8 ± 1	0.234	0.818
open arm time (%)	43 ± 8	35 ± 9	0.617	0.544
total arm entries (n)	23 ± 2	22 ± 3	0.106	0.917
Light/dark test				
latency to first entry into the lit area (s)	53 ± 13	71 ± 34	0.548	0.589
entries into the lit area (n)	16 ± 2	13 ± 2	1.174	0.253
time spent in the lit area (s)	167 ± 17	185 ± 29	0.568	0.576
distance traveled (cm)	2811 ± 200	2781 ± 273	0.568	0.576

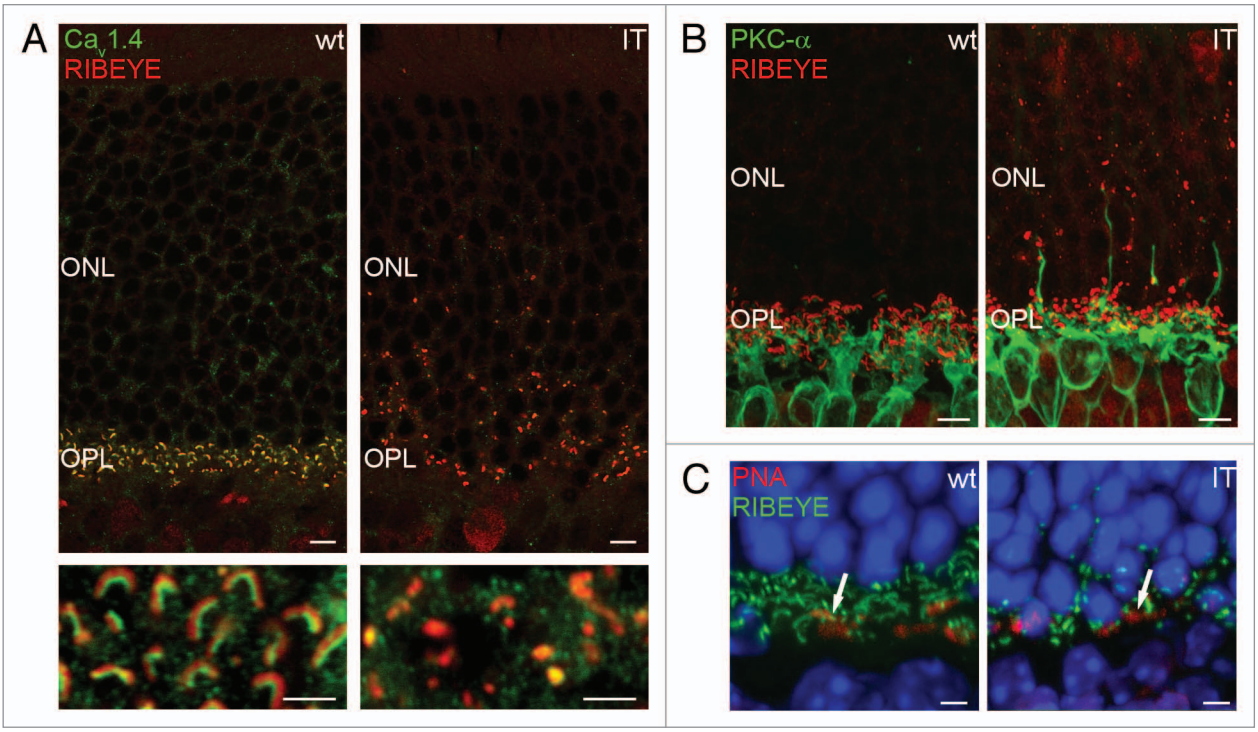

Figure 4. Photoreceptor synapses in adult wt and IT mice. (**A**) Immunofluorescence double-labeling of Cav1.4 (green) and the synaptic protein RIBEYE (red) in wt (right) and IT (left) mice. Wt mice show mature horseshoe-shaped ribbons whereas IT synapses were variable in morphology. (**B**) Co-staining with the rod bipolar cell maker PKCα (green) and CtBP2/Ribeye (red). Ectopic synapses in the outer nuclear layer (ONL) were observed only in IT mice (right). (**C**) Similar PNA staining (red) of cone synapses together with RIBEYE (green) in wt (left) and IT (right) mice. Scale bar 2 µm.

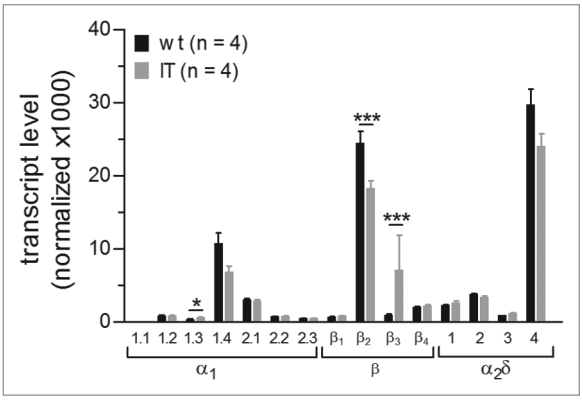

Figure 5. Expression profiles of voltage-activated Ca^{2+} channels in mouse retina of IT mice. The mRNA expression profiles of all high voltage-activated Ca^{2+} channel α_1, β, and $\alpha_2\delta$ subunit isoforms were determined in retinas of adult wt (black) and IT (gray) mice. Transcript levels (i.e., number of molecules per sample; see Material and Methods) of the individual experiments were normalized to the expression of the control genes Gapdh and Sdha. Log10 transformed transcript levels were analyzed by 2-way ANOVA: genotype, $F_{(1)} = 1.6$, $p = 0.208$; gene, $F_{(13)} = 131.5$, $p < 0.001$; genotype*gene, $F_{(13)} = 3.3$, $p < 0.001$; p values are derived from Holm-Sidak posthoc analysis. Data are presented as mean ± SEM. Note that in comparison to wt, expression of Cav1.4 trended to be less in IT mice ($p = 0.05$).

($p = 0.05$), β_2, and $\alpha_2\delta$-4 was evident in IT mice (**Fig. 5**). This finding may reflect a loss of photoreceptors, which was consistent also with our staining experiments (**Fig. 2**). In 2 out of 4 IT mice analyzed expression levels of the auxiliary β_3 subunit were 5-fold and 20-fold higher when compared with the other wt and IT mice, respectively (data not shown). This result is a plausible explanation for the highly significant increase of β_3 expression in IT mice ($p < 0.001$). Intriguingly, although transcripts for Cav1.3 account for only 2% of total α_1 subunits in wt they were significantly higher expressed in IT ($p = 0.03$). The isoforms Cav2.1, β_4 and $\alpha_2\delta$-2, which have previously been shown to be co-expressed in the cerebellum[25] also show comparable expression levels in the retina as implicated previously.[36]

Behavioral phenotype of IT mice

Finally, we investigated the role of Cav1.4 in visual function subjecting mice to established behavioral paradigms. Since these tests were all locomotion-based, we first screened for possible alterations in motor function. Wt and IT mice did not differ in novelty-induced locomotor activity (i.e., the distance traveled in the open field test and light/dark test or the total arm entries in the elevated plus maze test) as compared with wt (**Table 2**). Next, we assessed the visual performance of wt and IT mice subjecting them to the visual platform test of the Morris water maze[37] (**Fig. 6**). The escape latency (latency to reach and climb the platform) gradually decreased with the increasing number of trials performed (repeated measures ANOVA: $F(\text{trial})_{7,154} = 10.689$, $p < 0.001$) in both genotypes ($F(\text{trial} \times \text{genotype})_{7,154} = 0.445$, $p = 0.872$). However, in IT mice the latency was greatly

increased as compared with wt ($F(genotype)_{1,22}$ = 60.149, p < 0.001), pointing towards poor visual function of IT mice. In order to exclude a specific deficit in learning or memory-related processes as a cause for the impaired performance in the visible platform task of the Morris water maze, we tested the animals in an auditory cued fear-conditioning paradigm. Conditional responses, as indicated by freezing behavior, increased to the same extent in wt and IT mice upon 3 CS-footshock pairings (repeated measures ANOVA: $F(pairing)_{4,88}$ = 62.502, p < 0.001; $F(genotype)_{1,22}$ = 0.430, p = 0.519; $F(pairing \times genotype)_{4,88}$ = 0.6189, p = 0.650). On the next day in a novel context presentation of the CS alone did not elicit different freezing levels between the 2 genotypes suggesting normal learning capabilities of IT mice (percent freezing: wt 46.9 ± 5.5, IT 40.8 ± 5.2, t = 0.807, p = 0.428). Stimulated by human studies showing that the loss of vision has an impact on emotionality,[38,39,40] we also investigated the anxiety-related behavior of IT mice. No differences in any anxiety-related parameter including the entries into or time spent in the center of the open field, the latency, entries and time in the open arms of the elevated plus maze or the latency, entries into and time spent in the light compartment of the light/dark test were observed as compared with wt (**Table 2**).

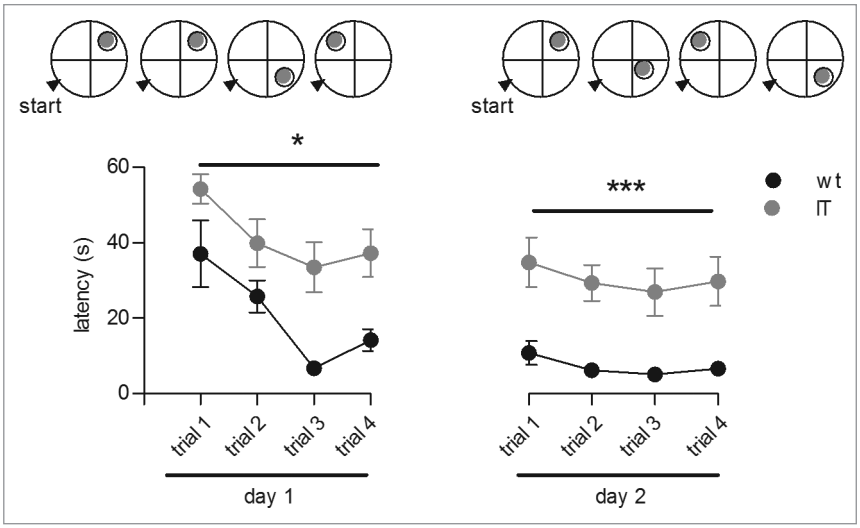

Figure 6. Behavioral phenotype of adult wt and IT mice. Performances of mice (latency to escape from the pool onto the platform) in the visible platform test of the Morris water maze task during 4 trials per day over 2 training days are shown. The fixed starting position of the mice is indicated by a black arrow while the varying positions of the platform are indicated by gray circles. Data represent the mean ± SEM; n = 13 for wt mice (black circles) and n = 11 for IT mice (gray circles). * p < 0.0.5 and *** p < 0.001 using a repeated-measures ANOVA and a post Fisher LSD test.

Discussion

Gain-of-function mutation I745T results in a loss of visual function

ERGs from Cav1.4 KO mice under scotopic and photopic conditions predicted a virtual lack of retinal transmission of electrical signals at the first synapse, affecting both rod and cone photoreceptors.[12] Recent data[33] also provided evidence that rod photoreceptor synapses in these mice remain immature which could inhibit photoreceptor synaptic transmission. Our data show that the level of synaptic maturation in adult IT mice, in contrast, was variable. Most synapses were abnormal, round, or elongated. However, some showed the horseshoe-like shape typical for mature wt synapses. In these cells specifically, a gain-of-function may limit the dynamic range of photoreceptor responses to an extent that would reduce but not completely suppress retinal signaling as seen in our ERG recordings. The marked leftward shift in the activation curve found in heterologously expressed IT channels[2] might increase the basal calcium levels in photoreceptors, due to higher activity at depolarized membrane potentials in the absence of light. Such high Ca^{2+} levels near the release sites could also lead to an increase in the time needed to shut-off glutamate release upon light exposure resulting in increased response latencies.

Our immunohistochemical data show cone anomalies similar to KO mice previously described.[33,41] Glypho, an enzyme that catalyzes the rate-limiting step in glycogenolysis (in brain but also retinal Müller glial cells and cones[42,43,44]) represents a main limited energy reserve.[45] The apparent stronger immunofluorescence signal in the cones and likely in surrounding cells in the IPL suggests that these cell types sense metabolic stress and show a higher need for glycogen breakdown. Although seen to a much lesser extent, the presence of potential degenerative signs is in line with a recent report on KO mice.[33]

The visually guided behavior tests supported our functional and structural findings. IT mice displayed increased escape latencies in the cued version of the Morris Water maze confirming poor visual ability. The performance of IT mice was comparable to that of animals with naturally occurring retinal degeneration including rd12 mice[37] and mice of the FVB/NJ, DBA/2, C3H, NIH Swiss and Black Swiss mice strains owen.[46,47] The Morris Water maze paradigm was used for assessing visual function.[48,49,50] Due to its primary field of application which is testing for spatial learning deficits in rodents[51] we wished to exclude the possibility that a cognitive deficit may underlie their bad performance. We therefore subjected wt and IT mice to an auditory cued fear-conditioning paradigm where vision is not essential. Indeed, both genotypes did not differ in fear learning or memory which is in line with other models of impaired vision owen.[46,52,53]

Additional information on retinal calcium channels obtained from the IT model

The expression profiling supported findings that Cav1.4 but also Cav1.3[5,54-63] and Cav1.2 [4,5] LTCCs are expressed in the retina. Interestingly, Cav1.3 channels were upregulated in IT. The retinal Cav1.3 distribution pattern is, however, controversial. Some studies showed accumulation in the inner segments of photoreceptors, OPL, INL, or GCL, whereas another reported Cav1.3

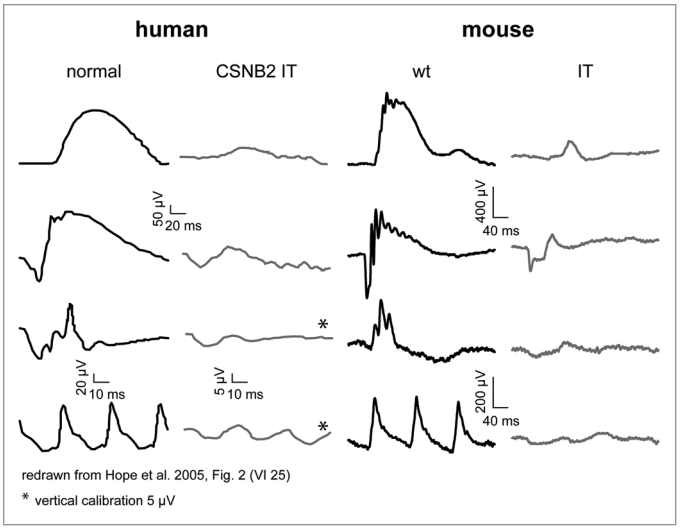

Figure 7. Functional comparison of human and murine subjects affected by the I745T mutation. Ganzfeld ERG recordings from a normal subject (left) and a patient with incomplete CSNB carrying the CACNA1F mutation I745T (center left) were redrawn form the original records (ref. 3). They correlate rather well with the murine data of wt (C57BL/6N; center right) and IT mice (right). The set of records follows the human ERG diagnostic standard as issued by the International Society for Clinical Electrophysiology of Vision (ISCEV; www.iscev.org/standards). From top to bottom, traces in each column represent the scotopic single flash response, the scotopic mixed response, the photopic single flash response, and the photopic 30 Hz flicker ERG. The murine records were obtained with identical paradigms.

expression across retinal cell layers.[5] Therefore, the role of Cav1.3 remains ambiguous. A contribution of Cav1.3 to ERG light peak regulation in the pigment retinal epithelium (RPE) is reported.[64] Though in our preparation the RPE was never included. Cav1.3 channels are also subject to rapid glutamate-induced internalization, likely to serve as a protective negative feedback mechanism[62] implying a role in other processes than synaptic transmission. Upregulation of Cav1.3 channels may be part of a potential compensatory mechanism in IT. The high level of expression of Cav2.1, β_4, and $\alpha_2\delta$-2 in IT retinas is intriguing. Although retinal pathway involvement in the adaptation mechanism to circadian phase-shift has been excluded previously in Cav2.1-mutated migraine mice[65] this hypothesis was never directly tested. The mammalian retina contains a clock that generates molecular circadian rhythms independent of the suprachiasmatic nucleus master clock,[66] but a calcium channel contribution was so far only reported for Cav1.2.[67,68]

IT mice serve as a good model for the functional phenotype seen in human patients

The Ganzfeld ERG recordings, both dark adapted (scotopic) and light adapted (photopic), suggest that there is a very close match between rod and cone system responses in CSNB2 patients carrying the I745T mutation[1] and the IT mouse line (**Fig. 7**). The functional pattern in both resembles a form of incomplete CSNB; rod and cone single flash responses as well as the flicker ERG were typically altered. The particular feature in I745T mutants, presumably associated with the gain-of-function nature of the disorder, is that the negative components of the scotopic standard flash response are smaller than those found in other CSNB types, but on the other hand a distinct remaining b-wave component is present. The comparison with the human data clearly underlines that the IT mouse line is a specific model for the functional phenotype seen in respective patients.

Materials and Methods

Animals

Animals were group-housed under standard laboratory conditions (12:12 light/dark cycle with lights on at 07:00 h, 22 ± 2 °C, 50–60% humidity) with pelleted food and water available ad libitum. All experiments were designed to minimize animal suffering as well as the number of animals used and were approved by the national ethical committee on animal care and use (Austrian Federal Ministry for Science and Research; BMWF-66.008/0016-II/3b/2012) and the Institutional Animal Care and Use Committee at the University of Iowa. Animals were killed by cervical dislocation in compliance with international laws and policies or by carbon dioxide exposure followed by cervical dislocation as approved by the Institutional Animal Care and Use Committee at the University of Iowa. All ERG and OCT procedures in animals were performed in accordance with the ARVO Statement for the Use of Animals in Ophthalmic and Vision Research with permission of local authorities (Regierungspräsidium Tübingen).

Cav1.4 mouse lines

We used a mouse model made by Dr Marion Maw (University of Otago) which carries the mutation I745T in the CACNA1F gene identified in a New Zealand CSNB2 family (IT).[4] Mouse tail biopsies were collected from all mice before and after the experiment for genotyping. Only male mice were investigated. Genomic DNA was isolated using buffer containing 10 mM Tris (pH 8.8), 50 mM KCl and 0.1% Triton X-100. We controlled for the IT allele and the corresponding wt alleles, as well as the rd8 mutant allele. IT mice were checked with following specific primers fwd-CACTCCAGACATCCTGCTGA and rev-GTCAACCCATGCTGTCTCCT. The PCR product for the wt allele has a length of 288-bp and the one for the IT allele 449-bp. PCR reaction was performed in a total volume of 20 µl, containing 2 µl DNA eluate, 0.2 µM fwd and rev primer, 0.025 U GoTaq DNA Polymerase (Promega), 1.5 mM MgCl, and 200 µM dNTPs. The following reaction cycle was used: 95 °C 4 min, 40 cycles of 9 5°C for 30 s, 63 °C for 30 s and 72 °C for 45 s, with a final extension at 72 °C for 10 min. Because the background of both IT and wt littermates as non-littermate wt controls was C57BL/6N we also genotyped for the rd8 mutation allele[13] which was amplified with fwd – CCCCTGTTTGCATGGAGGAAACTTGGAAG and rev-GCCCCATTTGCACACTGATGAC (224-bp product). The following PCR program was used for this assay: 94°C for 5 min, followed by 35 cycles at 94 °C for 30 s, 65 °C for 30 s, 72 °C for 30 s and a final elongation step of 72 °C for 7 min. The wt allele was amplified with fwd-GTGAAGACAGCTACAGTTCTGATC and rev-GCCCCATTTGCACACTGATGAC (220 bp product size). For the mutant allele

a PCR reaction of 25 µl was applied; containing 2 µl DNA, 1.6 µM forward and reverse primer, 0.02 U GoTaq DNA Polymerase (Promega), 1.2 mM MgCl and 100 µM dNTPs. The following PCR program was used: 94 °C for 5 min, followed by 35 cycles at 94 °C for 30 s, 65 °C for 30 s, 72 °C for 30 s. and a final elongation step of 72 °C for 7 min. The wt allele was amplified as follows: 25 µM reaction volume containing 2 µl DNA, 0.8 µM fwd primer and 1.6 µM rev primer, 0.02 U GoTaq DNA Polymerase (Promega), 1.2 mM MgCl, and 100 µM dNTPs. For the wt allele, DNA was denaturated at 94°C for 5 min, followed by 35 cycles of 94 °C for 30 s, 58 °C for 30 s, 72 °C for 30 s followed by extension at 72 °C for 7 min. Mice used in the study were either heterozygous or homozygous for the mutated allele; the wt retinal phenotype was without pathological findings.

Table 1. Markers investigated in immunofluorescence studies

Primary antibodies /markers	Dilution	Company
glycogen phosphorylase (glypho)	1:2000	Gift from Dr Hamprecht (Pfeiffer-Guglielmi et al., 2003)
sc-14363/blue sensitive cone opsin	1:200	Santa Cruz Biotechnology Inc. Heidelberg, Germany
biotinylated peanut agglutinin (PNA)	1:25	Vector Laboratories, California, USA
DAPI	1:10000	Sigma, St. Louis, MO
rabbit/mouse PKC-α	1:500	Santa Cruz, Dallas, Texas and Sigma, St. Louis, MO
rabbit/mouse RIBEYE	1:500	Covance, Princeton, NJ and BD bioscience, San Jose, CA
rabbit Cav1.4	1:1000	Custom-made (Dr Amy Lee)
Secondary antibodies		
Alexa Fluor® 488 Donkey Anti-Goat IgG	1:300 or 1:1000	Life Technologies, Grand Island, NY
Alexa Fluor ® 594 Goat Anti Guinea Pig IgH	1:300	Life Technologies, Grand Island, NY
Alexa Fluor ® 568-Goat Anti-mouse IgG	1:1000	Life Technologies, Grand Island, NY
Streptavidin, Alexa Fluor® 546 conjugate	1:300	Life Technologies, Grand Island, NY

Immunocytochemisty

Fixation and embedding

Eleven week old mice were sacrificed in the morning by cervical dislocation and decapitation. Eyes were removed, opened at the sclero-corneal rim and fixed for 15 min in 4% paraformaldehyde (PFA) in phosphate-buffered saline (PBS, 1 × , pH 7.4). After removal of cornea and lens, the eyecups were fixed for 2 h in 4% PFA/1 × PBS at room temperature (RT), rinsed in 1 × PBS (4 changes), and cryoprotected in increasing concentrations of sucrose (10% and 20% in 1 × PBS). Eyecups were embedded in a 1:1 mixture of 20% sucrose in 1x PBS and OCT medium (Tissue-Tek, Sakura) for 2 d at RT. Sections of 16 µm thickness were collected on to Superfrost Plus slides, air-dried for 24 h and stored at – 20°C until further use.

Immunofluoroescence

Sections were washed 3 times with washing buffer (1 × PBS, 0.1% Triton X-100, and 0.05% NaN_3). For primary antibody labeling or PNA, the tissue was blocked with 1% bovine serum albumin (BSA, Sigma) in 1 × PBS, 0.1% Triton X-100 and 0.05% NaN_3 for 30 min at RT. Primary antibody incubation and PNA staining was performed overnight at 4°C. Sections were washed 3 times in washing buffer, incubated with the secondary antibody for 1 h at RT, washed 3 times and counterstained with DAPI before mounting in Aqua-Poly/Mount (Polysciences). Primary and secondary antibodies and PNA were used in dilutions listed in **Table 1**. Micrographs or series of microsgraphs were taken with a Zeiss Axiovert 200M (Carl Zeiss). Images were adjusted for brightness and contrast and assembled using Photoshop CS5 (Adobe). Z-stacks were taken in 0.1 µm intervals and deconvolved with Huygens Essential (Scientific Volume Imaging B.V.) software. Processing of synaptic connections was done essentially as described previously.[14] In some experiments Hoechst stain (1:1000) was applied along with secondary antibodies. Confocal microscopy was performed using a Fluoview 1000 confocal microscope (Olympus) with 60X or 100X oil-immersion objectives or a Zeiss LSM710 confocal microscope with a Plan-Neofluar 63x/1.4 oil-immersion objective (Carl Zeiss). For consistency among figures, the red and green colors were switched using Adobe Photoshop.

Electroretinography

The functional implications of the I745T mutation was assessed in the IT mouse line in vivo with electroretinography (ERG). ERGs were recorded binocularly from animals at the age of 6 weeks postnatally as described previously.[15,16] Mice were anaesthetized using Ketamine (66.7 mg/kg body weight) and Xylazine (11.7 mg/kg body weight). Their pupils were dilated and single flash ERG responses were obtained under scotopic (dark-adapted overnight) and photopic (light-adapted with a background illumination of 30 cdm^{-2} starting 10 min before recording) conditions. Single white-flash stimuli ranged from – 4 to 1.5 log $cdsm^{-2}$ under dark-adapted and from – 2 to 1.5 log $cdsm^{-2}$ under light-adapted conditions. Ten responses were averaged with inter-stimulus intervals of 5 s (for – 4 to – 0.5 log $cdsm^{-2}$) or 17 s (for 0 to 1.5 log $cdsm^{-2}$). Responses to trains of flashes (flicker) were obtained under dark – adapted conditions using a fixed intensity (0.5 log $cdsm^{-2}$, resembling the International Society for Clinical Electrophysiology of Vision standard flash (ISCEV SF) intensity.[17] Flicker responses were averaged 30 times, and band-pass filter cut-off frequencies were 0.3 and 300 Hz for all ERG recordings. ERGs were obtained in n = 4 IT and n = 2 wt control animals.

Spectral Domain Optical Coherence Tomography

Spectral Domain Optical Coherence Tomography (SD-OCT) imaging was done with a commercially available Spectralis™ HRA+OCT device (Heidelberg Engineering) featuring a broadband superluminescent diode at 870 nm as low coherent light source. Each 2-dimensional B-scan recorded at 30° field of view consists of 1536 A-scans, which are acquired at a speed of 40000

scans per second. Optical depth resolution is approximately 7 μm with digital resolution reaching 3.5 μm. Imaging was performed using the proprietary software package Eye Explorer (version 3.2.1.0, Heidelberg Engineering). OCTs were recorded binocularly from animals at the age of 6 weeks postnatally as described previously.[18,19]

Quantitative RT-PCR

Whole retinas, brain and muscle from 8 week old wt and mutant mice were dissected. Tissue was collected and flash frozen in liquid nitrogen. For control PCRs, tsA-201 cells were transfected with cDNA encoding Cav1.4 (Accession number JF701915). Total RNA of either mouse retinas or transfected tsA-201 was isolated with RNeasy Plus Mini Kit, (Qiagen) with an extra purification step with RNase-Free DNase Set (Qiagen). For total RNA isolation of brain and muscle RNeasy Lipid Tissue Midi Kit or respectively muscle RNeasy Fibrous Tissue Midi Kit were used. cDNA synthesis was performed with RT-PCR first strand synthesis (Fermentas, ThermoScientific). For cDNA synthesis of retina, total RNA eluate, for muscle and brain 35ng/μl of RNA eluate was used. Qualitative PCRs were conducted using cDNA in the following range: retina 25 – 116 ngμl^{-1}, brain and muscle: 35 ngμl^{-1} and transfected cells 1.5 – 1.9 μgμl^{-1}. Specific primer for Cav1.1, 1.2, 1.4 as well as various splice forms of Cav1.3 were tested.[20,21,22,23,24] *Taqman RT-PCR* on cDNA obtained from retinas (see above) was performed according to a previously developed protocol.[25] The relative abundance of different Cav subunit transcripts was assessed by TaqMan quantitative PCR (qRT-PCR) using a standard curve method based on PCR products of known concentration in combination with normalization using the most stable control genes as previously described.[25] TaqMan gene expression assays specific for all high-voltage activated Ca^{2+} channel subunits (α_1, β, and $\alpha_2\delta$) were designed to span exon–exon boundaries, and were purchased from Applied Biosystems. The following assays were used [name (gene symbol), assay ID (Applied Biosystems)]: Cav1.1 (Cacna1s), Mm00489257_m1; Cav1.2 (Cacan1c), Mm00437953_m1; Cav1.3 (Cacna1d), Mm01209919_m1; Cav1.4 (Cacna1f), Mm00490443_m1; Cav2.1 (Cacna1a), Mm00432190_m1; Cav2.2 (Cacna1b), Mm00432226_m1; Cav2.3 (Cacna1e), Mm00494444_m1; β_1 (Cacnb1), Mm00518940_m1; β_2 (Cacnb2), Mm00659092_m1; β_3 (Cacnb3), Mm00432233_m1; β_4 (Cacnb4) Mm00521623_m1; $\alpha_2\delta$-1 (Cacna2d1), Mm00486607_m1; $\alpha_2\delta$-2 (Cacna2d2), Mm00457825_m1; $\alpha_2\delta$-3 (Cacna2d3), Mm00486613_m1; $\alpha_2\delta$-4 (Cacna2d4), Mm01190105_m1. The endogenous control genes included were [name (gene symbol), assay ID (Applied Biosystems)]: γ-cytoplasmic actin (ACTB), Mm00607939_s1; β-2-microglobulin (B2M), Mm00437762_m1; glyceraldehyde-3-phosphate dehydrogenase (GAPD), Mm99999915_g1; hypoxanthine phosphoribosyl-transferase 1 (HPRT1), Mm00446968_m1; succinate dehydrogenase complex, subunit A (SDHA), Mm01352363_m1; tata box binding protein (TBP), Mm00446973_m1; transferrin receptor (TFRC), Mm00441941_m1. The qRT-PCR (50 cycles) was performed in duplicates using 10–20 ng total RNA equivalents of cDNA and the specific TaqMan gene expression assay for each 20 μl reaction in TaqMan Universal PCR Master Mix (Applied Biosystems). Measurements were performed on four independent RNA preparations from each genotype. Analyses were performed using the 7500 Fast System (Applied Biosystems). The cycle threshold (Ct) values for each Cav gene expression assay were recorded for each individual preparation. To allow a direct comparison between the expression levels in different tissues, we normalized all experiments to Gapdh and Sdha, which were determined to be most stable expressed reference genes across all preparations and time points.[26] Subsequently normalized molecule numbers were calculated for each Cav subunit from their respective standard curve.[25]

Behavioral experiments

All behavioral experiments were performed between 09:00 and 14:00 h after the animals had been habituated to the testing room for at least 24 h. In order to decrease the number of animals used, the behavioral experiments, with at least 2 d of rest between each, were performed in the same animals in the following order: (1) animals were tested in the open field test,[27,28] light/dark test[28] and the elevated plus maze test,[5] (2) their visual function was assessed in a modified Morris water maze test involving a visible escape platform[5] and (3) auditory fear conditioning was used to assess (vision-independent) learning capabilities.[29]

Open field

Mice were individually placed into the periphery of an open field (41 × 41 × 41 cm, floor illumination 150 lx) whose area was divided into a 28 × 28 cm central zone. The entries into the central zone, the time spent in the central zone and the overall distance traveled by the mice were measured during the 10 min exploration time by using an automated activity monitoring system (TruScan, Coulbourn Instruments).

Light/dark test

The white, aversive compartment (41 × 20.5 × 41 cm, floor illumination 400 lx) and the dark, safe compartment (41 × 20.5 × 41 cm covered by a black top, floor illumination 10 lx) of the testing arena were connected by a small opening (7 × 7 cm) located in the center of the partition at floor level. Animals were individually placed into the dark compartment facing away from the opening and allowed to freely explore the apparatus for 10 min. The latency to the first entry into the lit compartment, the number of entries and time spent in the lit compartment and the overall distance traveled by each mouse was automatically registered (TruScan, Coulbourn Instruments).

Elevated plus maze test

The 5 min test was performed on a plus-shaped maze which was elevated (73 cm) from the floor and consisted of 2 open arms (à 30 × 6 cm; 100 lx), two closed arms (à 30 × 6 × 17 cm; illuminated with red light), and a central neutral zone (6 × 6 cm). Animals were placed onto the neutral zone of the maze facing a closed arm and their locomotor behavior was continuously recorded by a tracking system (TSE Technical and Scientific Equipment GmbH) connected to a camera positioned above the maze. The latency to the first open arm entry, the number of open arm entries, the percentage of time spent on the open arms and the distance traveled were analyzed.

Visible platform test of the Morris water maze

Mice were placed into a circular pool (1.2 min in diameter) filled with water (23 °C) and illuminated at 40 lx. Starting from a fixed position they were allowed to escape by climbing onto a platform (10 cm diameter) placed just above the water and marked with a flag for facilitating visualization. The animals were allowed to stay on the platform for additional 10 s. In case the animal was not able to locate the platform, it was gently guided to it by the experimenter. On each of 2 consecutive days animals performed four 60 s trials separated by 60 min. The location of the platform was changed after each trial. The latency to reach the platform was recorded.

Auditory fear conditioning

In the conditioning context (25 × 25 × 30 cm chamber with transparent walls and a metal rod floor cleaned with water, floor illumination 300 lx; TSE) mice received three pairings (2 min inter-pairing interval) of an auditory 30 s white noise conditioned stimulus (CS; 10 kHz, 80 dB) and a co-terminating 2 s mild foot shock (0.6 mA). Twenty-four hours after the auditory fear conditioning 3 CSs separated by 5 s were presented to mice for a fear expression test in a novel context (25 × 25 × 30 cm chamber with black walls and a solid gray cleaned with ethanol, floor illumination 10 lx; TSE). The time remaining in freezing behavior during the CS presentations was manually determined by an observer blind to the genotype.

Statistics

All values are presented as mean ± SEM for the indicated number of experiments (n). For multiple comparisons of in vitro data statistical significance was determined by a 1-way analysis of variance (ANOVA) followed by Bonferroni multiple-comparison or the Dunnett post-hoc test. For comparisons of 2 groups, data were analyzed by the Student t test as indicated for individual experiments. Behavioral data were statistically analyzed using repeated-measures ANOVA followed by post Fisher's LSD test or the unpaired Student t test. In qRT-PCR experiments, data were organized and analyzed using MS Excel and SigmaStat (Systat Software, Inc.) statistical software. Statistical significance was determined on log10 transformed expression levels using 2-way-ANOVA followed by Holm-Sidak posthoc comparison. Statistical significance was set at $p < 0.05$.

Disclosure of Potential Conflicts of Interest

No potential conflicts of interest were disclosed.

Acknowledgments

We thank Stefanie Geisler and Stefan Kummer for excellent technical assistance and Peter Ahnelt for helpful discussions. This work was supported by the Austrian Science Fund (FWF P-22528 to Koschak A), SFB F44 (F4402 to Koschak A, F4406 to Obermair GJ), P24079-B21 (to Obermair GJ) the German Research Council DFG (Se837/6–2), the National Institutes of Health (DC009433 and HL87120 to Lee A, DC010362 [Iowa Center for Molecular Auditory Neuroscience], EY020542 to Baker SA) and the Medical University Vienna.

References

1. Hope CI, Sharp DM, Hemara-Wahanui A, Sissingh JI, Lundon P, Mitchell EA, Maw MA, Clover GM. Clinical manifestations of a unique X-linked retinal disorder in a large New Zealand family with a novel mutation in CACNA1F, the gene responsible for CSNB2. Clin Experiment Ophthalmol 2005; 33:129-36; PMID:15807819; http://dx.doi.org/10.1111/j.1442-9071.2005.00987.x
2. Hemara-Wahanui A, Berjukow S, Hope CI, Dearden PK, Wu SB, Wilson-Wheeler J, Sharp DM, Lundon-Treweek P, Clover GM, Hoda JC, et al. A CACNA1F mutation identified in an X-linked retinal disorder shifts the voltage dependence of Cav1.4 channel activation. Proc Natl Acad Sci U S A 2005; 102:7553-8; PMID:15897456; http://dx.doi.org/10.1073/pnas.0501907102
3. Morgans CW. Localization of the alpha(1F) calcium channel subunit in the rat retina. Invest Ophthalmol Vis Sci 2001; 42:2414-8; PMID:11527958
4. Specht D, Wu SB, Turner P, Dearden P, Koentgen F, Wolfrum U, Maw M, Brandstätter JH, tom Dieck S. Effects of presynaptic mutations on a postsynaptic Cacna1s calcium channel colocalized with mGluR6 at mouse photoreceptor ribbon synapses. Invest Ophthalmol Vis Sci 2009; 50:505-15; PMID:18952919; http://dx.doi.org/10.1167/iovs.08-2758
5. Busquet P, Nguyen NK, Schmid E, Tanimoto N, Seeliger MW, Ben-Yosef T, Mizuno F, Akopian A, Striessnig J, Singewald N. CaV1.3 L-type Ca2+ channels modulate depression-like behaviour in mice independent of deaf phenotype. Int J Neuropsychopharmacol 2010; 13:499-513; PMID:19664321; http://dx.doi.org/10.1017/S1461145709990368
6. Mercer AJ, Chen M, Thoreson WB. Lateral mobility of presynaptic L-type calcium channels at photoreceptor ribbon synapses. J Neurosci 2011; 31:4397-406; PMID:21430141; http://dx.doi.org/10.1523/JNEUROSCI.5921-10.2011
7. Koschak A, Reimer D, Walter D, Hoda JC, Heinzle T, Grabner M, Striessnig J. Cav1.4alpha1 subunits can form slowly inactivating dihydropyridine-sensitive L-type Ca2+ channels lacking Ca2+-dependent inactivation. J Neurosci 2003; 23:6041-9; PMID:12853422
8. Stockner T, Koschak A. What can naturally occurring mutations tell us about Ca(v)1.x channel function? Biochim Biophys Acta 2013; 1828:1598-607; PMID:23219801; http://dx.doi.org/10.1016/j.bbamem.2012.11.026
9. McRory JE, Hamid J, Doering CJ, Garcia E, Parker R, Hamming K, Chen L, Hildebrand M, Beedle AM, Feldcamp L, et al. The CACNA1F gene encodes an L-type calcium channel with unique biophysical properties and tissue distribution. J Neurosci 2004; 24:1707-18; PMID:14973233; http://dx.doi.org/10.1523/JNEUROSCI.4846-03.2004
10. Hoda JC, Zaghetto F, Koschak A, Striessnig J. Congenital stationary night blindness type 2 mutations S229P, G369D, L1068P, and W1440X alter channel gating or functional expression of Ca(v)1.4 L-type Ca2+ channels. J Neurosci 2005; 25:252-9; PMID:15634789; http://dx.doi.org/10.1523/JNEUROSCI.3054-04.2005
11. Peloquin JB, Rehak R, Doering CJ, McRory JE. Functional analysis of congenital stationary night blindness type-2 CACNA1F mutations F742C, G1007R, and R1049W. Neuroscience 2007; 150:335-45; PMID:17949918; http://dx.doi.org/10.1016/j.neuroscience.2007.09.021
12. Mansergh F, Orton NC, Vessey JP, Lalonde MR, Stell WK, Tremblay F, Barnes S, Rancourt DE, Bech-Hansen NT. Mutation of the calcium channel gene Cacna1f disrupts calcium signaling, synaptic transmission and cellular organization in mouse retina. Hum Mol Genet 2005; 14:3035-46; PMID:16155113; http://dx.doi.org/10.1093/hmg/ddi336
13. Mattapallil MJ, Wawrousek EF, Chan CC, Zhao H, Roychoudhury J, Ferguson TA, Caspi RR. The Rd8 mutation of the Crb1 gene is present in vendor lines of C57BL/6N mice and embryonic stem cells, and confounds ocular induced mutant phenotypes. Invest Ophthalmol Vis Sci 2012; 53:2921-7; PMID:22447858; http://dx.doi.org/10.1167/iovs.12-9662
14. Haeseleer F, Imanishi Y, Maeda T, Possin DE, Maeda A, Lee A, Rieke F, Palczewski K. Essential role of Ca2+-binding protein 4, a Cav1.4 channel regulator, in photoreceptor synaptic function. Nat Neurosci 2004; 7:1079-87; PMID:15452577; http://dx.doi.org/10.1038/nn1320
15. Seeliger MW, Zrenner E, Apfelstedt-Sylla E, Jaissle GB. Identification of Usher syndrome subtypes by ERG implicit time. Invest Ophthalmol Vis Sci 2001; 42:3066-71; PMID:11687556
16. Tanimoto N, Muehlfriedel RL, Fischer MD, Fahl E, Humphries P, Biel M, Seeliger MW. [Landmark Ed]. Front Biosci 2009; 14:2730-7; http://dx.doi.org/10.2741/3409
17. Marmor MF, Holder GE, Seeliger MW, Yamamoto S; International Society for Clinical Electrophysiology of Vision. Standard for clinical electroretinography (2004 update). Doc Ophthalmol 2004; 108:107-14; PMID:15455793; http://dx.doi.org/10.1023/B:DOOP.0000036793.44912.45

18. Fischer MD, Huber G, Beck SC, Tanimoto N, Muehlfriedel R, Fahl E, Grimm C, Wenzel A, Remé CE, van de Pavert SA, et al. Noninvasive, in vivo assessment of mouse retinal structure using optical coherence tomography. PLoS One 2009; 4:e7507; PMID:19838301; http://dx.doi.org/10.1371/journal.pone.0007507
19. Huber G, Beck SC, Grimm C, Sahaboglu-Tekgoz A, Paquet-Durand F, Wenzel A, Humphries P, Redmond TM, Seeliger MW, Fischer MD. Spectral domain optical coherence tomography in mouse models of retinal degeneration. Invest Ophthalmol Vis Sci 2009; 50:5888-95; PMID:19661229; http://dx.doi.org/10.1167/iovs.09-3724
20. Koschak A, Obermair GJ, Pivotto F, Sinnegger-Brauns MJ, Striessnig J, Pietrobon D. Molecular nature of anomalous L-type calcium channels in mouse cerebellar granule cells. J Neurosci 2007; 27:3855-63; PMID:17409250; http://dx.doi.org/10.1523/JNEUROSCI.4028-06.2007
21. Singh A, Gebhart M, Fritsch R, Sinnegger-Brauns MJ, Poggiani C, Hoda JC, Engel J, Romanin C, Striessnig J, Koschak A. J Biol Chem 2008
22. Sinnegger-Brauns MJ, Huber IG, Koschak A, Wild C, Obermair GJ, Einzinger U, Hoda JC, Sartori SB, Striessnig J. Expression and 1,4-dihydropyridine-binding properties of brain L-type calcium channel isoforms. Mol Pharmacol 2009; 75:407-14; PMID:19029287; http://dx.doi.org/10.1124/mol.108.049981
23. Baig SM, Koschak A, Lieb A, Gebhart M, Dafinger C, Nürnberg G, Ali A, Ahmad I, Sinnegger-Brauns MJ, Brandt N, et al. Loss of Ca(v)1.3 (CACNA1D) function in a human channelopathy with bradycardia and congenital deafness. Nat Neurosci 2011; 14:77-84; PMID:21131953; http://dx.doi.org/10.1038/nn.2694
24. Bock G, Gebhart M, Scharinger A, Jangsangthong W, Busquet P, Poggiani C, Sartori S, Mangoni ME, Sinnegger-Brauns MJ, Herzig S, et al. Functional properties of a newly identified C-terminal splice variant of Cav1.3 L-type Ca2+ channels. J Biol Chem 2011; 286:42736-48; PMID:21998310; http://dx.doi.org/10.1074/jbc.M111.269951
25. Schlick B, Flucher BE, Obermair GJ. Voltage-activated calcium channel expression profiles in mouse brain and cultured hippocampal neurons. Neuroscience 2010; 167:786-98; PMID:20188150; http://dx.doi.org/10.1016/j.neuroscience.2010.02.037
26. Willems E, Leyns L, Vandesompele J. Standardization of real-time PCR gene expression data from independent biological replicates. Anal Biochem 2008; 379:127-9; PMID:18485881; http://dx.doi.org/10.1016/j.ab.2008.04.036
27. Singewald N, Sinner C, Hetzenauer A, Sartori SB, Murck H. Magnesium-deficient diet alters depression – and anxiety-related behavior in mice—influence of desipramine and Hypericum perforatum extract. Neuropharmacology 2004; 47:1189-97; PMID:15567428; http://dx.doi.org/10.1016/j.neuropharm.2004.08.010
28. Sartori SB, Whittle N, Hetzenauer A, Singewald N. Magnesium deficiency induces anxiety and HPA axis dysregulation: modulation by therapeutic drug treatment. Neuropharmacology 2012; 62:304-12; PMID:21835188; http://dx.doi.org/10.1016/j.neuropharm.2011.07.027
29. Sartori SB, Hauschild M, Bunck M, Gaburro S, Landgraf R, Singewald N. Enhanced fear expression in a psychopathological mouse model of trait anxiety: pharmacological interventions. PLoS One 2011; 6:e16849; PMID:21386891; http://dx.doi.org/10.1371/journal.pone.0016849
30. Blanks JC, Johnson LV. Specific binding of peanut lectin to a class of retinal photoreceptor cells. A species comparison. Invest Ophthalmol Vis Sci 1984; 25:546-57; PMID:6715128
31. Johnson LV, Hageman GS. Enzymatic characterization of peanut agglutinin-binding components in the retinal interphotoreceptor matrix. Exp Eye Res 1987; 44:553-65; PMID:3109930; http://dx.doi.org/10.1016/S0014-4835(87)80163-X
32. Haverkamp S, Wässle H, Duebel J, Kuner T, Augustine GJ, Feng G, Euler T. The primordial, blue-cone color system of the mouse retina. J Neurosci 2005; 25:5438-45; PMID:15930394; http://dx.doi.org/10.1523/JNEUROSCI.1117-05.2005
33. Zabouri N, Haverkamp S. Calcium channel-dependent molecular maturation of photoreceptor synapses. PLoS One 2013; 8:e63853; PMID:23675510; http://dx.doi.org/10.1371/journal.pone.0063853
34. Wycisk KA, Budde B, Feil S, Skosyrski S, Buzzi F, Neidhardt J, Glaus E, Nürnberg P, Ruether K, Berger W. Structural and functional abnormalities of retinal ribbon synapses due to Cacna2d4 mutation. Invest Ophthalmol Vis Sci 2006; 47:3523-30; PMID:16877424; http://dx.doi.org/10.1167/iovs.06-0271
35. Ball SL, McEnery MW, Yunker AM, Shin HS, Gregg RG. Distribution of voltage gated calcium channel β subunits in the mouse retina. Brain Res 2011; 1412:1-8; PMID:21831364
36. Kamphuis W, Hendriksen H. Expression patterns of voltage-dependent calcium channel alpha 1 subunits (alpha 1A-alpha 1E) mRNA in rat retina. Brain Res Mol Brain Res 1998; 55:209-20; PMID:9582423; http://dx.doi.org/10.1016/S0169-328X(97)00363-X
37. Pang JJ, Chang B, Kumar A, Nusinowitz S, Noorwez SM, Li J, Rani A, Foster TC, Chiodo VA, Doyle T, et al. Gene therapy restores vision-dependent behavior as well as retinal structure and function in a mouse model of RPE65 Leber congenital amaurosis. Mol Ther 2006; 13:565-72; PMID:16223604; http://dx.doi.org/10.1016/j.ymthe.2005.09.001
38. Fenwick E, Rees G, Pesudovs K, Dirani M, Kawasaki R, Wong TY, Lamoureux E. Social and emotional impact of diabetic retinopathy: a review. Clin Experiment Ophthalmol 2012; 40:27-38; PMID:21575125; http://dx.doi.org/10.1111/j.1442-9071.2011.02599.x
39. Kempen GI, Zijlstra GA. Clinically Relevant Symptoms of Anxiety and Depression in Low-Vision Community-Living Older Adults. Am J Geriatr Psychiatry 2013; PMID:23567435; http://dx.doi.org/10.1016/j.jagp.2012.08.007
40. Renieri G, Pitz S, Pfeiffer N, Beutel ME, Zwerenz R. Changes in quality of life in visually impaired patients after low-vision rehabilitation. Int J Rehabil Res 2013; 36:48-55; PMID:22890293; http://dx.doi.org/10.1097/MRR.0b013e328357885b
41. Raven MA, Orton NC, Nassar H, Williams GA, Stell WK, Jacobs GH, Bech-Hansen NT, Reese BE. Early afferent signaling in the outer plexiform layer regulates development of horizontal cell morphology. J Comp Neurol 2008; 506:745-58; PMID:18076080; http://dx.doi.org/10.1002/cne.21526
42. Ignacio PC, Baldwin BA, Vijayan VK, Tait RC, Gorin FA. Brain isozyme of glycogen phosphorylase: immunohistological localization within the central nervous system. Brain Res 1990; 529:42-9; PMID:2282504; http://dx.doi.org/10.1016/0006-8993(90)90809-P
43. Nihira M, Anderson K, Gorin FA, Burns MS. Primate rod and cone photoreceptors may differ in glucose accessibility. Invest Ophthalmol Vis Sci 1995; 36:1259-70; PMID:7775103
44. Pfeiffer-Guglielmi B, Francke M, Reichenbach A, Fleckenstein B, Jung G, Hamprecht B. Glycogen phosphorylase isozyme pattern in mammalian retinal Müller (glial) cells and in astrocytes of retina and optic nerve. Glia 2005; 49:84-95; PMID:15390095; http://dx.doi.org/10.1002/glia.20102
45. Osorio-Paz I, Sánchez-Chávez G, Salceda R. Control of glycogen content in retina: allosteric regulation of glycogen synthase. PLoS One 2012; 7:e30822; PMID:22363495; http://dx.doi.org/10.1371/journal.pone.0030822
46. Owen EH, Logue SF, Rasmussen DL, Wehner JM. Assessment of learning by the Morris water task and fear conditioning in inbred mouse strains and F1 hybrids: implications of genetic background for single gene mutations and quantitative trait loci analyses. Neuroscience 1997; 80:1087-99; PMID:9284062; http://dx.doi.org/10.1016/S0306-4522(97)00165-6
47. Clapcote SJ, Lazar NL, Bechard AR, Roder JC. Effects of the rd1 mutation and host strain on hippocampal learning in mice. Behav Genet 2005; 35:591-601; PMID:16184487; http://dx.doi.org/10.1007/s10519-005-5634-5
48. O'Steen WK, Spencer RL, Bare DJ, McEwen BS. Analysis of severe photoreceptor loss and Morris water-maze performance in aged rats. Behav Brain Res 1995; 68:151-8; PMID:7654301; http://dx.doi.org/10.1016/0166-4328(94)00168-F
49. Spencer RL, O'Steen WK, McEwen BS. Water maze performance of aged Sprague-Dawley rats in relation to retinal morphologic measures. Behav Brain Res 1995; 68:139-50; PMID:7654300; http://dx.doi.org/10.1016/0166-4328(94)00167-E
50. Koch S, Sothilingam V, Garcia Garrido M, Tanimoto N, Becirovic E, Koch F, Seide C, Beck SC, Seeliger MW, Biel M, et al. Gene therapy restores vision and delays degeneration in the CNGB1(-/-) mouse model of retinitis pigmentosa. Hum Mol Genet 2012; 21:4486-96; PMID:22802073; http://dx.doi.org/10.1093/hmg/dds290
51. D'Hooge R, De Deyn PP. Applications of the Morris water maze in the study of learning and memory. Brain Res Brain Res Rev 2001; 36:60-90; PMID:11516773; http://dx.doi.org/10.1016/S0165-0173(01)00067-4
52. Bolivar VJ, Pooler O, Flaherty L. Inbred strain variation in contextual and cued fear conditioning behavior. Mamm Genome 2001; 12:651-6; PMID:11471061; http://dx.doi.org/10.1007/s003350020039
53. Clapcote SJ, Lazar NL, Bechard AR, Wood GA, Roder JC. NIH Swiss and Black Swiss mice have retinal degeneration and performance deficits in cognitive tests. Comp Med 2005; 55:310-6; PMID:16158906
54. Taylor WR, Morgans C. Localization and properties of voltage-gated calcium channels in cone photoreceptors of Tupaia belangeri. Vis Neurosci 1998; 15:541-52; PMID:9685206; http://dx.doi.org/10.1017/S0952523898153142
55. Morgans CW, El Far O, Berntson A, Wässle H, Taylor WR. Calcium extrusion from mammalian photoreceptor terminals. J Neurosci 1998; 18:2467-74; PMID:9502807
56. Morgans CW. Calcium channel heterogeneity among cone photoreceptors in the tree shrew retina. Eur J Neurosci 1999; 11:2989-93; PMID:10457194; http://dx.doi.org/10.1046/j.1460-9568.1999.00719.x
57. Firth SI, Morgan IG, Boelen MK, Morgans CW. Localization of voltage-sensitive L-type calcium channels in the chicken retina. Clin Experiment Ophthalmol 2001; 29:183-7; PMID:11446465; http://dx.doi.org/10.1046/j.1442-9071.2001.00401.x
58. Welch NC, Wood S, Jollimore C, Stevens K, Kelly ME, Barnes S. High-voltage-activated calcium channels in Muller cells acutely isolated from tiger salamander retina. Glia 2005; 49:259-74; PMID:15472989; http://dx.doi.org/10.1002/glia.20113
59. Cristofanilli M, Mizuno F, Akopian A. Disruption of actin cytoskeleton causes internalization of Ca(v)1.3 (alpha 1D) L-type calcium channels in salamander retinal neurons. Mol Vis 2007; 13:1496-507; PMID:17893673

60. Henderson D, Doerr TA, Gottesman J, Miller RF. Calcium channel immunoreactivity in the salamander retina. Neuroreport 2001; 12:1493-9; PMID:11388436; http://dx.doi.org/10.1097/00001756-200105250-00039
61. Xiao H, Chen X, Steele EC Jr. Abundant L-type calcium channel Ca(v)1.3 (alpha1D) subunit mRNA is detected in rod photoreceptors of the mouse retina via in situ hybridization. Mol Vis 2007; 13:764-71; PMID:17563731
62. Mizuno F, Barabas P, Krizaj D, Akopian A. Glutamate-induced internalization of Ca(v)1.3 L-type Ca(2+) channels protects retinal neurons against excitotoxicity. J Physiol 2010; 588:953-66; PMID:20123787; http://dx.doi.org/10.1113/jphysiol.2009.181305
63. Kersten F, van Wijk E, van Reeuwijk J, van der Zwaag B, Maerker T, Peters T, Katsanis N, Wolfrum U, Keunen J, Roepman R, et al. Invest Ophthalmol Vis Sci 2009; PMID:19959638
64. Wu J, Marmorstein AD, Striessnig J, Peachey NS. Voltage-dependent calcium channel CaV1.3 subunits regulate the light peak of the electroretinogram. J Neurophysiol 2007; 97:3731-5; PMID:17376851; http://dx.doi.org/10.1152/jn.00146.2007
65. van Oosterhout F, Michel S, Deboer T, Houben T, van de Ven RC, Albus H, Westerhout J, Vansteensel MJ, Ferrari MD, van den Maagdenberg AM, et al. Enhanced circadian phase resetting in R192Q Cav2.1 calcium channel migraine mice. Ann Neurol 2008; 64:315-24; PMID:18825664; http://dx.doi.org/10.1002/ana.21418
66. Storch KF, Paz C, Signorovitch J, Raviola E, Pawlyk B, Li T, Weitz CJ. Intrinsic circadian clock of the mammalian retina: importance for retinal processing of visual information. Cell 2007; 130:730-41; PMID:17719549; http://dx.doi.org/10.1016/j.cell.2007.06.045
67. Ko ML, Liu Y, Shi L, Trump D, Ko GY. Circadian regulation of retinoschisin in the chick retina. Invest Ophthalmol Vis Sci 2008; 49:1615-21; PMID:18385082; http://dx.doi.org/10.1167/iovs.07-1189
68. Shi L, Ko ML, Ko GY. Rhythmic expression of microRNA-26a regulates the L-type voltage-gated calcium channel alpha1C subunit in chicken cone photoreceptors. J Biol Chem 2009; 284:25791-803; PMID:19608742; http://dx.doi.org/10.1074/jbc.M109.033993